Journal of Power Sources 205 (2012) 108–113

Contents lists available at SciVerse ScienceDirect

Journal of Power Sources

journal homepage: www.elsevier.com/locate/jpowsour

Use of anode barrier layers in tubular solid-oxide fuel cells for robust operation on hydrocarbon fuels

Wade A. Rosensteel[a], Sean M. Babiniec[a], Daniel D. Storjohann[a], Joshua Persky[b], Neal P. Sullivan[a,*]

[a] Mechanical Engineering Department, Colorado School of Mines, Golden, CO 80401, USA
[b] Protonex Technology Corporation, 153 Northboro Road, Southborough, MA 01772-1034, USA

ARTICLE INFO

Article history:
Received 2 November 2011
Received in revised form
21 December 2011
Accepted 1 January 2012
Available online 11 January 2012

Keywords:
SOFC
Biogas
Internal reforming
Barrier layer
Diffusion barrier
Direct hydrocarbon operation
CPOX
Steam reforming

ABSTRACT

This paper presents a unique demonstration of anode barrier-layer technology in a tubular solid-oxide fuel cell (SOFC) architecture. The anode barrier layer is a chemically inert, porous ceramic tube that is positioned within the inside diameter of the tubular SOFC, separating the catalytically active anode from the hydrocarbon-carrying fuel stream. This porous tube reduces the respective diffusion rates of reactants and products into and out of the anode. This increases the local concentration of electrochemically produced steam and carbon dioxide throughout the anode, resulting in higher local steam-to-carbon ratios that enhance the selectivity of internal-reforming reactions toward hydrogen and carbon monoxide over the formation of deleterious carbon deposits. In this study, stable electrochemical performance is demonstrated under a simulated "biogas" fuel stream (63% CH_4/34% CO_2/3% H_2O) over 12 days of continuous operation. The performance of the barrier layer-equipped SOFC is characterized under biogas and hydrogen fuels, and compared to the performance of an SOFC without a barrier layer. While some decrease in power density is evident with the presence of a barrier layer, the performance decrease at 0.7 V is modest. Morphological characterization after performance testing reveals no evidence of carbon deposition within the anode or barrier layer. These results demonstrate the potential of barrier-layer technology in tubular solid-oxide fuel cell architectures.

1. Introduction

This paper presents a unique application of anode barrier-layer technology in a tubular solid-oxide fuel cell (SOFC) architecture. The anode barrier layer (Fig. 1) is a chemically inert, porous ceramic tube that is positioned within the inside diameter of the tubular SOFC, separating the catalytically active anode from the hydrocarbon fuel stream. This porous tube acts to reduce the respective diffusion rates of reactants and products into and out of the anode. This increases the local concentration of electrochemically produced steam within the porous anode structure, and higher local steam-to-carbon ratios that enhance the selectivity of internal-reforming reactions toward hydrogen and carbon monoxide over the formation of deleterious carbon deposits. By promoting steam-reforming reactions over solid-carbon reactions, the barrier layer widens the safe operating windows of hydrocarbon-fueled solid-oxide fuel cells.

Stable SOFC operation under hydrocarbon fuels is well documented [1–6], and remains one of the most desirable attributes of high-temperature solid-oxide fuel cells. In typical ceramic–metallic composite anode supports, comprised of yttria-stabilized zirconia and nickel, direct operation on hydrocarbon fuels is enabled through nickel-catalyzed steam-reforming reactions between the supplied fuel and steam generated through electrochemical reactions underway at the triple-phase boundaries. As shown in the inset of Fig. 1, steam diffuses from the anode–electrolyte interface through the porous anode support to the fuel channel, encountering and catalytically reacting with hydrocarbon fuels that counter-diffuse into the anode support from the fuel channel. Many catalytic reactions on the nickel surface are possible between the steam and hydrocarbon reactants; higher local steam-to-carbon ratios enable a high selectivity to hydrogen, carbon monoxide, and carbon dioxide, and reduce the likelihood of deleterious carbon-deposit formation [5–8]. Solid-carbon formation within the anode reduces the number of catalytically active nickel sites, and eventually causes fracture and catastrophic failure of the membrane-electrode assembly (MEA).

A common strategy for using hydrocarbon fuels with solid-oxide fuel cells is to reform (or partially reform) the fuel to syngas ($CO/CO_2/H_2$) upstream of the SOFC using a steam reformer or catalytic-partial-oxidation reactor [9]. Upstream reforming widens the deposit-free operating windows for the SOFC, but adds balance-of-plant hardware and cost, and reduces both cell and system efficiency [9]. Alternatively, a portion of the hot anode-exhaust

* Corresponding author. Tel.: +1 303 273 3656; fax: +1 303 273 3602.
E-mail address: nsulliva@mines.edu (N.P. Sullivan).

0378-7753/$ – see front matter © 2012 Elsevier B.V. All rights reserved.
doi:10.1016/j.jpowsour.2012.01.035

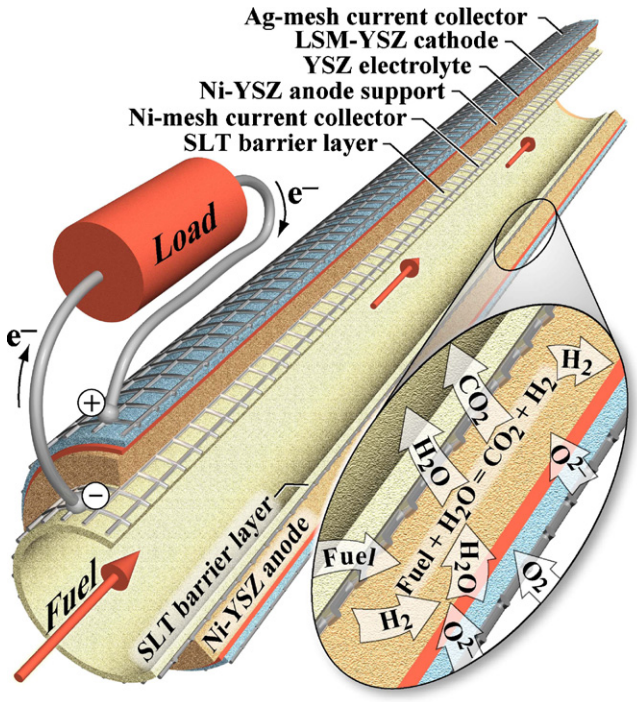

Fig. 1. Illustration of an anode-supported tubular SOFC equipped with a barrier layer. An inset illustrates steam reforming of a hydrocarbon fuel within the anode support.

gases may be recycled to increase product concentrations in the anode [10–13]. This approach requires a high-temperature blower to re-circulate exhaust gas, for which development remains a challenge [9].

Lin et al. [14,15], have shown the effectiveness of anode barrier layers or, "diffusion barriers," for widening the operating windows for hydrocarbon fuels in small, planar, "button-cell" SOFC configurations. "Integrated-planar" or "segmented-in-series" architectures also present an example of barrier-layer technology in which the support structure acts as a barrier layer [16,17]. Computational modeling by Zhu et al. [9] has suggested competitive performance for a barrier-layer design in comparison to an anode-recycle design, as the barrier-layer design requires only a single pass of fuel. Model results also show that the barrier-layer architecture results in a more-uniform thermal profile over the length of the tubular SOFC, reducing the potential for hot or cold spots near the SOFC inlet. The maximum power density is decreased due to increased gas-transport losses induced by a barrier layer [9], but at fairly modest levels, highlighting the more-uniform current density over the length of the SOFC that is a result of the barrier-layer architecture. While these results from Zhu et al. [9] show the promise that anode barrier-layer technology holds for tubular SOFCs, demonstrations to date have been limited to planar button-cell configurations [14,15].

This study integrates barrier-layer technology into a tubular solid-oxide fuel cell architecture, with continuous operation demonstrated on a simulated "biogas" fuel stream. Biogas is a byproduct of the anaerobic-digestion processing that is commonly utilized for bio-remediation of solid wastes, and is widely used at municipal wastewater-treatment plants (WWTPs). The composition of biogas can vary substantially across facilities [18,19], but primarily consists of methane and carbon dioxide, with trace amounts of steam, oxygen, and nitrogen, and ppm-levels of contaminants [20]. These contaminants (e.g. sulfur-containing species, siloxanes, etc. [21–24]) can be removed with commercially available gas-cleaning technologies, resulting in a composition of approximately 65 mol% CH_4 and 35 mol% CO_2.

A large wastewater-treatment facility (~200 million gallons per day) may continuously generate 15 MW of this low-quality methane stream (based on the higher-heating value of CH_4), presenting a considerable opportunity for electricity generation. Conversion of WWTP-generated biogas presents an ideal application of fuel-cell technology. Both the WWTP electric loads and the biogas-generation rate are fairly consistent, minimizing the load-following requirements of the electric generator. Indeed, many molten-carbonate and phosphoric acid fuel-cell systems have been installed at WWTPs [20,24–26].

Solid-oxide fuel cells offer advantages in comparison to these conversion methods due to their higher electrical efficiency, internal-reforming capability, opportunity for co-generation of high-quality waste heat, and potential for low system cost. Though solid-oxide fuel cell operation on biogas has been demonstrated [5,6,27–33], carbon-deposit formation has proven to be problematic. This work seeks in part to address deposit-formation issues through use of barrier-layer technology, as described subsequently.

2. Materials and methods

In this study, a tubular solid-oxide fuel cell (Protonex Technology Corp.) is equipped with a chemically inert porous barrier layer following the assembly approach shown in Fig. 1. The Protonex SOFC utilizes materials that are fairly common in the SOFC community; the anode is a ceramic–metallic composite comprised of nickel and 8-mol% yttria-stabilized zirconia (YSZ), and provides mechanical support for the device. The electrolyte also utilizes YSZ, and the cathode is a composite of lanthanum strontium manganate (LSM) and YSZ. The outside diameter of the cell is 10.3 mm, and the cathode length is 16.0 mm, corresponding to a 5.18 cm^2 active area.

The barrier layer that is placed within the inner diameter of the tubular cell is comprised of 80 wt.% lanthanum-doped strontium titanate ($Sr_{0.8}La_{0.2}TiO_3$ – SLT, Fuelcellmaterials.com) and 20 wt.% YSZ (Tosoh). SLT and YSZ are essentially chemically inert with respect to biogas fuel; other inert porous ceramic materials could also be utilized. While SLT displays a modest electronic conductivity [34,35], this materials-performance feature is not harnessed in this tubular barrier-layer fuel-cell assembly. Current collection is accomplished using nickel and silver mesh on the anode and cathode, respectively, as shown in Fig. 1.

The porous, tubular barrier layer is formed from a slurry composed of a SLT–YSZ oxide suspension using a binary combination of pore formers. The slurry composition is shown in Table 1. The pore formers include a 1:1 mixture of carbon black (Cabot, Vulcan XC72R) and 6-μm-diameter poly(methyl methacrylate) beads (PMMA, Calibre CA-6, Microbeads). The total amount of pore former added is 30 vol.% of oxide.

An oxide-PMMA suspension is dispersed separately from a carbon-black suspension. This separate dispersion prevents the

Table 1
Slip cast formulation.

Chemical	Purpose	Quantity
De-ionized water	Oxide solvent	40 vol.%
Oxide (SLT/YSZ)	Oxide	60 vol.%
Darvan C	Dispersant	4 wt.% of oxide
PMMA	Pore former	15 vol.% of oxide
Deionized water	Carbon black solvent	5× wt.% of carbon black
Carbon black	Pore former	15 vol.% of oxide
PVP10	Carbon black dispersant	5 wt.% of carbon black
PEG	Binder	1.5 wt.% of oxide

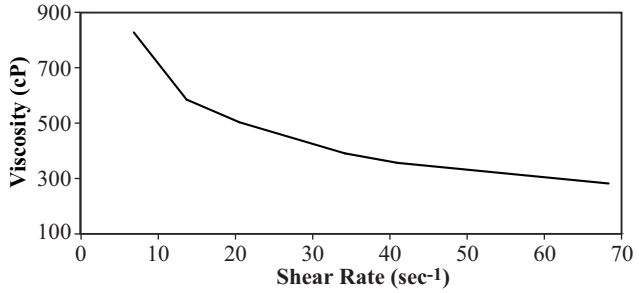

Fig. 2. Viscosity of SLT–YSZ anode-support slip at 25 °C.

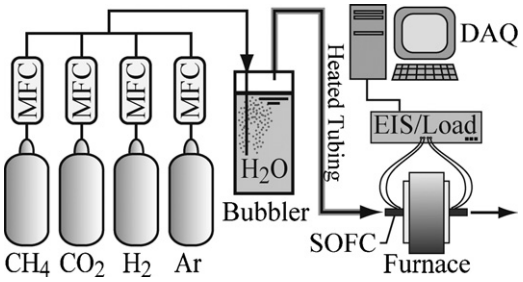

Fig. 3. Process flow diagram of SOFC electrochemical test station.

oxide phase from adsorbing and stripping dispersant from the carbon black; such stripping can result in an unstable suspension that is not suitable for casting. The dispersant for the oxide-PMMA suspension is ammonium polymethacrylate in water (Darvan C, R.T. Vanderbilt Company), and the dispersant for the carbon-black suspension is polyvinylpyrrolidone (PVP-10, Sigma–Aldrich). These suspensions are ball-milled separately for 12 h, after which they are combined and ball-milled for another 24 h. The slurry formulation, as shown in Table 1, is fairly standard [36], except for the ratio of oxide dispersant to oxide, which is about three times more than what is theoretically required for stable dispersion. The excess oxide dispersant provides greater particle surface coverage, which prevents the oxide-PMMA suspension from affecting the stability of the carbon-black suspension.

A binary combination of pore formers allows for a robust fabrication process. If PMMA is used alone as a pore former, problems arise during sintering; the polymer transitions into a glassy, viscous phase before burnout that may lead to significant part deformation during sintering. Alternately, dispersing a sufficient amount of carbon black to act as a solitary pore former is difficult, and leads to problems with slurry stability. An unstable slurry may cause cracking in the slip-cast part during drying, prior to high-temperature sintering. These problems are avoided while fabricating a high porosity SLT–YSZ barrier layer with the use of a binary combination of PMMA and carbon-pore formers.

The viscosity of the slip is measured with a Brookfield LVDVE115 viscometer, using the #62 spindle. Fig. 2 shows the viscosity of the cast slip over a range of shear rates. The non-linear response indicates non-Newtonian, shear-thinning behavior that is typical of colloidal suspensions. At higher shear rates, the viscosity approaches 300 cP, which is acceptable for slip casting [37].

Prior to casting, the slip is placed in a vacuum chamber for an hour to remove air bubbles. The slip is mixed on a stir plate until it can be poured into a porous plaster mold, where it is allowed to set for 5 min. The remaining slip is removed from the mold, and the green part is allowed to dry overnight within the mold.

The resulting part is released from the mold, and sintered in a furnace (DelTech DT-29-TH-M-10-E2404). The sintering profile includes a 3-h polymer-burnout step at 300 °C, with high-temperature sintering at 1475 °C for 1 h. Modest heating and cooling rates ($\leq$3 °C min^{-1}) are utilized throughout the sintering process. The resulting tubular barrier layer has an outside diameter of 6.40 mm, and a wall thickness of 0.55 mm. Open porosity is 38% with fairly fine pores of about 0.6 μm in diameter, as measured through mercury porosimetry (Micromeritics AutoPore IV 9500).

The SLT barrier layer is then wrapped with a Ni-mesh current collector (100 × 100 mesh, Unique Wire Weaving, Inc.), and inserted into the 8.3 mm inside diameter of the SOFC. Cathode current-collection is accomplished by painting the cathode with Ag-paste, and wrapping it with 20-gauge Ag-wire. The SOFC assembly is then manifolded to alumina tubes using alumina paste (Cotronics Resbond 989FS) for sealing and mechanical support at operating temperatures.

The performance of the barrier-layer-equipped solid-oxide fuel cell is quantified under hydrogen and biogas fuels. For comparison, the performance of a similar Protonex SOFC without a barrier layer is also characterized, as described subsequently.

3. Electrochemical performance testing

The operation of tubular SOFCs with and without barrier-layer structures is characterized using an electrochemical test stand. A process flow diagram of the test apparatus is presented in Fig. 3. After installation of the SOFC assembly into the test stand, the assembly is heated in a furnace (Applied Test Systems) at a modest ramp rate of 1 °C min^{-1} to an operating temperature of 850 °C under a humidified forming gas fuel stream (94% Ar/3% H_2/3% H_2O). Humidification is achieved by passing the forming gas through a room-temperature bubbler. The fuel and temperature conditions are held constant for about 6 h, until stable electrochemical performance is observed, indicating that the electronically insulative nickel(II) oxide within the anode has been reduced to nickel.

After reduction, SOFC performance is first measured under humidified hydrogen fuel (97% H_2/3% H_2O). This initial performance under hydrogen fuel is used as a benchmark for cell performance; additional performance measurements under H_2 fuel are taken after operation under biogas in order to observe cell degradation.

After completing initial experiments under hydrogen fuel, humidified biogas (63% CH_4/34% CO_2/3% H_2O) is synthesized and fed to the SOFC assembly. Gas flow rates are maintained using Hastings Teledyne mass flow controllers (MFC); flow rates are sufficiently high to prevent any significant decrease in fuel concentration along the axial length of the cell. Such “flooded” conditions provide a rigorous coking test, as the concentration of electrochemically produced steam is fairly low, potentially favoring carbon-forming over syngas-forming reactions within the Ni–YSZ anode support. High fuel-utilization conditions can result in elevated steam concentrations within the anode support that could cause deleterious re-oxidation of the nickel phase. Such conditions are not examined as part of this work.

Polarization characterization is conducted using a Chroma 6130 electronic load, interfaced with National Instruments LabView software. A Gamry FC350 impedance analyzer and a TDI Dynaload RBL488 electronic load are utilized for electrochemical impedance spectroscopy (EIS) measurements.

After electrochemical performance testing, the Protonex SOFC and barrier layer are examined using electron microscopy for observance of carbon deposition. Analysis is carried out using an FEI Quanta 600i environmental scanning electron microscope (SEM), with energy-dispersive X-ray spectroscopy (EDX) capability.

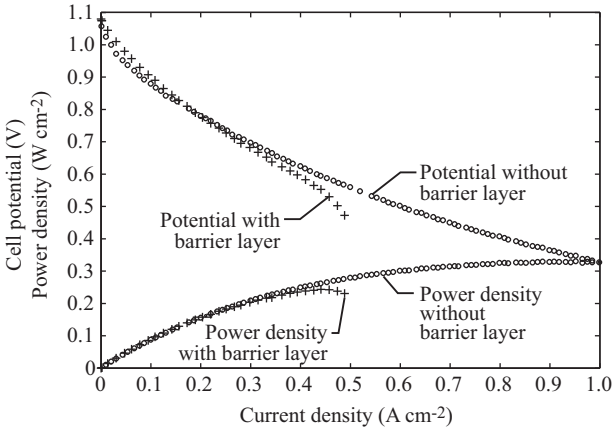

Fig. 4. Electrochemical performance of a tubular SOFC with and without an inert barrier layer. Fuel is humidified hydrogen under flooded conditions; operating temperature is 850 °C.

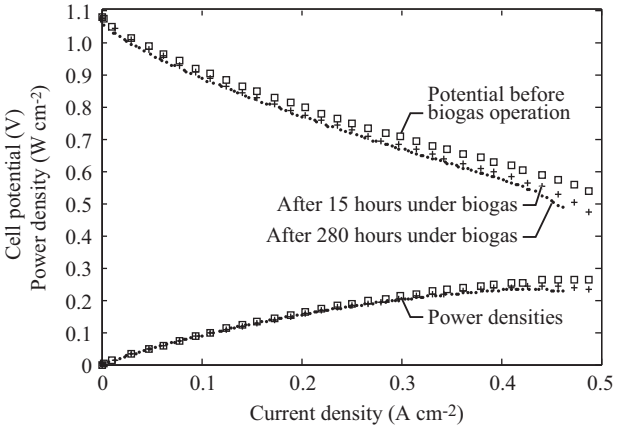

Fig. 6. Barrier-layer-equipped SOFC polarization before and after biogas operation, using humidified hydrogen fuel at 850 °C.

4. Results and discussion

4.1. Performance and stability

Stable electrochemical performance is observed after approximately 6 h of operation under humidified forming gas fuel. Fig. 4 compares the performance of tubular SOFCs under hydrogen fuel with and without a barrier-layer structure in place. The presence of the barrier layer within the tubular SOFC is found to reduce electrochemical performance; the maximum power density decreases from 0.331 W cm^{-2} to 0.264 W cm^{-2}. However, at a more-practical cell potential of 0.7 V, the power density is found to decrease only slightly (less than 7%), from 0.208 W cm^{-2} to 0.193 W cm^{-2}. These results indicated that overpotentials due to gas-transport become significant in the barrier-layer-equipped SOFC at current densities that are significantly lower than found in the conventional architecture. As the barrier layer is intended to increase the concentration of exhaust products in the anode, it consequently decreases the rate that fuel is transported into the anode, increasing concentration polarization. While this can be substantial at high overpotentials, the decrease in performance appears to be modest at a cell potential of 0.7 V.

The operational stability of the barrier-layer-equipped SOFC is investigated with galvanostatic endurance tests; results are shown in Fig. 5. Reasonably stable performance is demonstrated at 0.20 A cm^{-2} over 160 h (~6.7 days) of operation. The current density is then reduced to 0.15 A cm^{-2}; stable operation is again observed over an additional 50 h (2.1 days). Finally, current density is further reduced to 0.10 A cm^{-2}, with stable operation observed over an additional 70 h (2.9 days) of operation.

Operation at lower current densities increases the likelihood of deposit formation; the generation rate of electrochemically produced steam and CO_2 is directly proportional to the current density, so the fuel in the anode is less diluted with products at lower current densities. Despite the low current densities shown in Fig. 5, degradation in cell potential is found to be quite modest: 0.0085, 0.0130, and 0.0086% h^{-1} at 0.20, 0.15, and 0.10 A cm^{-2}, respectively.

Performance degradation is also quantified during the 280 h of biogas operation by periodically switching the fuel stream from simulated biogas to humidified hydrogen, and measuring polarization characteristics. Results are displayed in Fig. 6. After 15 h of biogas operation, the maximum power density under humidified hydrogen fuel degrades from 0.264 to 0.244 W cm^{-2}. After 280 h, the maximum power is reduced to 0.233 W cm^{-2}. The power density at a potential of 0.7 V degrades 11.6% from 0.215 to 0.190 W cm^{-2} after 15 h of biogas operation, and after 280 h, is reduced another 1.6 % to 0.187 W cm^{-2}. While this performance degradation is far from negligible, it does not appear to be due to deposit formation within the anode support, as evidenced by the electron micrographs shown in the following section.

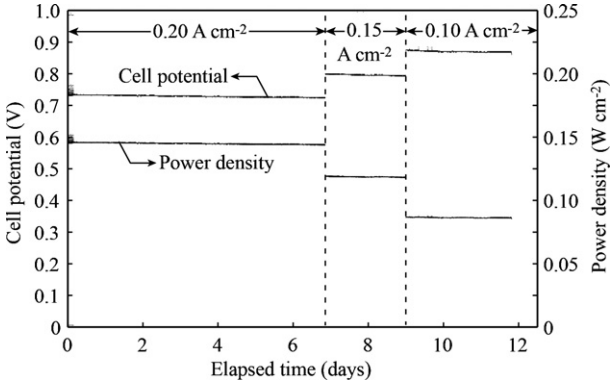

Fig. 5. SOFC stability over twelve days of operation under biogas fuel.

4.2. Electrochemical impedance spectroscopy

Electrochemical impedance spectroscopy is utilized to compare the physical and chemical processes underway while operating on humidified hydrogen and biogas fuels. The electrical impedance spectrums for a barrier layer equipped SOFC operating on each fuel are shown in Fig. 7. Measurements are performed using a Gamry FC350 impedance analyzer and a TDI Dynaload RBL488 electronic load.

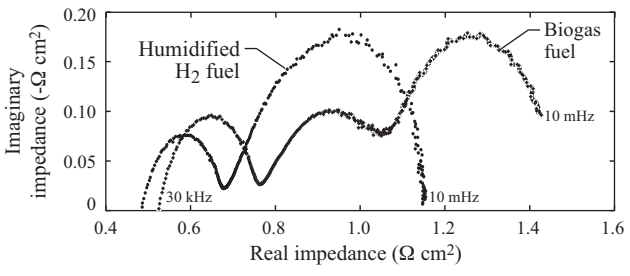

Fig. 7. Nyquist plots during biogas operation and hydrogen operation at 850 °C and 0.10 A cm^{-2}.

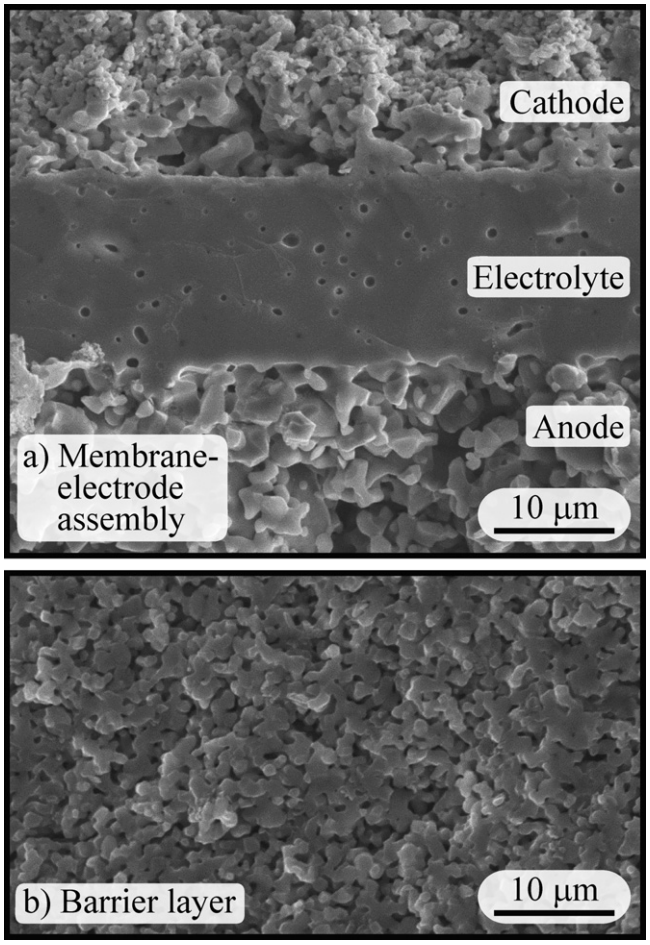

Fig. 8. Electron micrographs of fracture cross-sections after 280 h of operation on biogas fuel, and 900 total hours of operation; (a) membrane-electrode assembly and (b) barrier layer. No carbon-deposit formation is observed in either image.

The high frequency intercepts in Fig. 7 correspond to ohmic losses in the SOFC, which are dominated by ion transport through the electrolyte. Ohmic losses are found to increase slightly under biogas operation. This is attributed to decreases in local cell temperature due to the endothermicity of methane internal-reforming reactions. This temperature decrease leads to slightly lower ionic conductivity in the YSZ electrolyte, and a modest increase in ohmic loss.

An additional arc is present at frequencies less than 150 mHz in Fig. 7 during biogas operation that is not present during hydrogen operation. Kromp et al. [38] were the first to report this process for a reformate-fuelled solid-oxide fuel cell. The process is attributed to the coupling of the water–gas shift reaction and gas-phase transport within the anode, and is precisely modeled as a resistor and a quasi-capacitor circuit element in a parallel arrangement.

4.3. Morphological characterization

After 900 h of performance testing, the tubular SOFC/barrier-layer assembly is cooled to room temperature, removed from the test stand and fractured. High-resolution electron micrographs of the fracture cross sections are shown in Fig. 8. The micrographs and EDX measurements (not shown) reveal no evidence of carbon deposition within the Ni–YSZ anode support or the barrier layer.

5. Conclusions

This paper demonstrates a unique integration of barrier-layer technology into a tubular solid-oxide fuel cell architecture. An inert, porous barrier layer comprised of lanthanum-doped strontium titanate (SLT) and yttria-stabilized zirconia (YSZ) is inserted within the inner diameter of an anode-supported, tubular solid-oxide fuel cell comprised of a Ni–YSZ anode, YSZ electrolyte, and LSM–YSZ cathode. Stable operation is observed over 280 h of operation at 850 °C under humidified biogas fuel (63% CH_4/34% CO_2/3% H_2O). Performance degradation is found to be modest (on the order of 0.01% h^{-1}) at a current density as low as 0.10 A cm^{-2}. The performance of the barrier-layer-equipped SOFC is characterized under biogas and hydrogen fuels, and compared to the performance of an SOFC without a barrier layer. While some decrease in power density is evident due to the presence of the barrier layer, the performance decrease at 0.7 V is limited. Morphological characterization after performance testing reveals no sign of carbon-deposit formation. These results demonstrate the potential of barrier-layer technology in tubular solid-oxide fuel cell architectures.

Acknowledgments

We gratefully acknowledge Prof. Robert J. Kee for fruitful discussions on internal reforming in solid-oxide fuel cells, and for provision of the illustration shown in Fig. 1. We also thankfully acknowledge Alexander Kromp for interpretation of electrochemical impedance spectroscopy data. Colorado School of Mines efforts are supported by the United States Department of Energy, Office of Energy Efficiency and Renewable Energy, under contract DE-EE-0000260.

References

[1] J. Liu, S.A. Barnett, Solid State Ionics 158 (2003) 11–16.
[2] C. Xia, F. Chen, M. Liu, Electrochem. Solid-State Lett. 4 (2001) A52–A54.
[3] J.B. Wang, J.-C. Jang, T.-J. Huang, J. Power Sources 122 (2002) 122–131.
[4] A. Weber, B. Sauer, A.C. Müller, D. Herbstritt, E. Ivers-Tiffée, Solid State Ionics 152–153 (2002) 543–550.
[5] Y. Shiratori, T. Oshima, K. Sasaki, Int. J. Hydrogen Energy 33 (2008) 6313–6321.
[6] Y. Shirator, K. Sasaki, J. Power Sources 180 (2008) 738–741.
[7] K. Sasaki, Y. Teraoka, J. Electrochem. Soc. 150 (2003) A878–A884.
[8] S. Assabumrungrat, N. Laosiripojana, P. Piroonlerkgul, J. Power Sources 159 (2006) 1274–1282.
[9] H. Zhu, A.M. Colclasure, R.J. Kee, Y. Lin, S.A. Barnett, U. Bossel (Eds.), Seventh European SOFC Forum, 2006, pp. B0704–B0760.
[10] A.A. Burke, L.G. Carreiro, J. Power Sources 158 (2006) 428–435.
[11] R.J. Braun, S.A. Klein, D.T. Reindl, J. Power Sources 158 (2006) 1290–1305.
[12] Y. Yi, A.D. Rao, J. Brouwer, G.S. Samuelsen, J. Power Sources 144 (2005) 67–76.
[13] W. Zhang, E. Croiset, P.L. Douglas, M.W. Fowler, E. Entchev, Energ. Convers. Manage. 46 (2005) 181–186.
[14] Y. Lin, Z. Zhan, S.A. Barnett, J. Power Sources 158 (2006) 1313–1316.
[15] Y. Lin, Z. Zhan, J. Liu, S.A. Barnett, Solid State Ionics 176 (2005) 1827–1835.
[16] F.J. Gardner, M.J. Day, N.P. Brandon, M.N. Pashley, M. Cassidy, J. Power Sources 86 (2000) 122–129.
[17] T.S. Lai, J. Liu, S.A. Barnett, Electrochem. Solid-State Lett. 7 (4) (2004) A78–A81.
[18] M. Kymälä inen, K. Lähde, M. Arnold, J.M. Kurola, M. Romantschuk, H. Kautola, J. Environ. Manage. (2011), doi:10.1016/j.jenvman.2011.01.003.
[19] V. Cigolotti, S. McPhail, A. Moreno, S.P. Yoon, J.H. Han, S.W. Nam, T.-H. Lim, Int. J. Hydrogen Energy 36 (2011) 10311–10318.
[20] R.J. Spiegel, J.L. Preston, J. Power Sources 86 (2000) 283–288.
[21] K. Haga, S. Adachi, Y. Shiratori, K. Itoh, K. Sasaki, Solid State Ionics 179 (2008) 1427–1431.
[22] M. Nourot, Experience with a desiccant siloxane removal system, WasteCon, Solid Waste Association of North America, Tampa, FL, USA, 2008.
[23] S.P. Hernández, F. Scarpa, D. Fino, R. Conti, Int. J. Hydrogen Energy 36 (2011) 8112–8118.
[24] D. Deublein, A. Steinhauser, Biogas from Waste and Renewable Resources, 2nd ed., Wiley-VCH, Weinheim, 2011.
[25] M. Bischoff, J. Power Sources 160 (2006) 842–845.
[26] M. Krumbeck, T. Klinge, B. Döding, J. Power Sources 157 (2006) 902–905.
[27] J. Staniforth, K. Kendall, J. Power Sources 71 (1998) 275–277.
[28] M. Jenne, T. Zähringer, A. Schuler, G. Piskay, D. Moos, Sulzer HEXIS SOFC Systems for Biogas and Heating Oil, European Fuel Cell Forum, 2002.
[29] J. Staniforth, K. Kendall, J. Power Sources 86 (2000) 401–403.

[30] J. Van herle, Y. Membrez, O. Buchel, J. Power Sources 127 (2004) 300–312.
[31] K. Girona, J. Laurencin, M. Petitjean, J. Fouletier, F. Lefebvre-Joud, ECS Trans. 25 (2009) 1041–1050.
[32] Y. Shiratori, T. Ijichi, T. Oshima, K. Sasaki, ECS Trans. 25 (2009) 1051–1060.
[33] M. Noponen, T. Hottinen, WFC20 Biogas Unit Operation, European Fuel Cell Forum, 2010.
[34] M.J. Escudero, J.T.S. Irvine, L. Daza, J. Power Sources 192 (2009) 43–50.
[35] K. Ahn, S. Jung, J.M. Vohs, R.J. Gorte, Ceram. Int. 33 (2007) 1065–1070.
[36] M.N. Rahaman, Ceramic Processing, Taylor and Francis, New York, 2007.
[37] P.J. Howard, A.C. Hughes, J. Mater. Sci. 35 (1999) 4827–4832.
[38] A. Kromp, A. Leonide, A. Weber, E. Ivers-Tiffée, J. Electrochem. Soc 158 (2011) B980–B986.